

# Intermolecular interactions in crystal structure, Hirshfeld surface, characterization, DFT and thermal analysis of 5-((5-bromo-1*H*-indol-3-yl)methylene)-1,3-dimethylpyrimidine-2,4,6(1*H*,3*H*,5*H*)-trione indole

Assem Barakat <sup>a, \*\*</sup>, Saied M. Soliman <sup>b, c</sup>, Hazem A. Ghabbour <sup>d, e</sup>, M. Ali <sup>a</sup>, Abdullah Mohammed Al-Majid <sup>a</sup>, Abdelkader Zarrouk <sup>f</sup>, Ismail Warad <sup>g, \*</sup>

<sup>a</sup> Department of Chemistry, College of Science, King Saud University, P. O. Box 2455, Riyadh 11451, Saudi Arabia

<sup>b</sup> Department of Chemistry, Rabigh College of Science and Art, P. O. Box 344, Rabigh, 21911, Saudi Arabia

<sup>c</sup> Department of Chemistry, Faculty of Science, Alexandria University, P.O. Box 426, Ibrahimia, Alexandria 21321, Egypt

<sup>d</sup> Department of Pharmaceutical Chemistry, College of Pharmacy, King Saud University, P.O. Box 2457, Riyadh 11451, Saudi Arabia

<sup>e</sup> Department of Medicinal Chemistry, Faculty of Pharmacy, Mansoura University, Mansoura 35516, Egypt

<sup>f</sup> LCAE-URAC18, Faculté des Sciences d'Oujda, Université Mohammed Premier, BP 4808, 60046 Oujda, Morocco

<sup>g</sup> Department of Chemistry, Science College, An-Najah National University, P.O. Box 7, Nablus, Palestine

## ARTICLE INFO

### Article history:

Received 19 December 2016

Received in revised form

9 February 2017

Accepted 10 February 2017

Available online 11 February 2017

### Keywords:

Condensation reaction

Barbituric acid

Indole

DFT-Computation

XRD

## ABSTRACT

Condensation reaction of 5-bromo-1*H*-indole-3-carbaldehyde and 1,3-dimethylpyrimidine-2,4,6(1*H*,3*H*,5*H*)-trione in ethanol under reflux conditions furnished the formation of 5-((5-bromo-1*H*-indol-3-yl)methylene)-1,3-dimethylpyrimidine-2,4,6(1*H*,3*H*,5*H*)-trione indole in a very good yield. The desired compound is characterized by spectroscopic and thermal tools, additionally the structure was confirmed by X-ray single crystal diffraction. Visually analysis of desired crystal structure using Hirshfeld surface revealed several short intermolecular connections on the molecule surface while the 2D fingerprint draw evaluated the atom-to-atom interactions percentages.

The structures of the monomer and the dimer of the product that are obtained from the B3LYP/6-31G(d,p) molecular geometry optimizations were compared with the XRD experimental one. Electronic spectra are assigned on the basis of the TD-DFT results and the molecular orbital (MO) energy level diagrams showing the different MOs included in these transitions are explored. The electrophilic and nucleophilic regions are shown using molecular electrostatic potential map. The GIAO method is used to compute and compare the NMR chemical shifts. The desired organic compound revealed a good thermal stability up to 215 °C.

© 2017 Elsevier B.V. All rights reserved.

## 1. Introduction

Derivatives of barbituric acid are important members of the pyrimidine family, many barbituric acid derivatives are known to possess a wide range of activities, such as hypnotics [1–3].

Indole derivatives constitute an important class of therapeutic agents in medicinal chemistry including anticancer [4], antioxidant

\* Corresponding author.

\*\* Corresponding author.

E-mail addresses: [ambarakat@ksu.edu.sa](mailto:ambarakat@ksu.edu.sa) (A. Barakat), [warad@najah.edu](mailto:warad@najah.edu) (I. Warad).

[5], anti-rheumatoid and anti-HIV [6,7] and also play a vital role in the immune system [8,9]. Many indole derivatives are considered as the most potent scavenger of free radicals [5]. Artificial receptors for biologically active molecules have attracted attention from the viewpoint of molecular recognition [10]. It was envisaged that the two pharmacophores if linked together (Scheme 1) would generate novel molecular templates, which are likely to exhibit interesting biological properties in animal models.

Combination of the Indoles, and barbituric acids leads to biological significance including anti-inflammatory, anti-hypnotic, anticancer, anti-convulsant agents and other application as agrochemicals [11–18].

Owing to the importance and in continuation of our work on

synthesis of biologically active compounds [19–21], we focused on the investigation of the chemical structure of 5-((5-bromo-1H-indol-3-yl)methylene)-1,3-dimethylpyrimidine-2,4,6(1H,3H,5H)-trione.

## 2. Experimental

### 2.1. General remarks

X-ray crystal structure analysis collected on a Bruker APEX-II D8 Venture area diffractometer. The NMR spectra were run in deuterated dimethyl sulfoxide (DMSO- $d_6$ ) using Jeol-400 NMR spectrometer.

#### 2.1.1. Synthesis of the desired compound: 5-((5-Bromo-1H-indol-3-yl)methylene)-1,3-dimethylpyrimidine-2,4,6(1H,3H,5H)-trione

The completeness of condensation reaction was monitored by TLC. A mixture of 5-bromo-1H-indole-3-carbaldehyde (1 mmol) and 1,3-dimethylpyrimidine-2,4,6(1H,3H,5H)-trione in 10 mL of EtOH in presence of piperidine (0.5 mmol) was stirred for 1 h under reflux, the product was filtrated, washed with 2 mL of cold EtOH and dried to give the desired compound. Further crystallization by slow diffusion of a solution in DCM/EtOH in Et<sub>2</sub>O to provide a single crystal suitable for X-ray diffraction analysis.

(Yield 86%); m.p. > 250 °C; <sup>1</sup>H NMR (400 MHz, DMSO- $d_6$ )  $\delta$ : 3.46 (s, 6H, 2\*CH<sub>3</sub>), 3.08 (s, 3H, ANCH<sub>3</sub>), 7.46 (d, 1H,  $J = 1.5$ , Indole), 7.55 (d, 1H,  $J = 1.5$ , Indole), 8.01 (s, 1H, Indole), 8.69 (s, 1H, Indole), 9.50 (s, 1H, CH=C), 12.86 (bs, 1H,  $J = 1.5$ , NH); <sup>13</sup>C NMR (100 MHz, DMSO- $d_6$ )  $\delta$ : 151.03, 149.35, 138.29, 134.61, 129.77, 125.34, 122.88, 120.38, 115.69, 110.02, 104.31, 102.22, 101.00, 22.38, 21.09; IR (KBr, cm<sup>-1</sup>)  $\nu_{\max} = 3225, 1688, 1675, 1550, 1445, 1265$ ; [Anal. Calcd.-for C<sub>15</sub>H<sub>12</sub>BrN<sub>3</sub>O<sub>3</sub>: C, 49.74; H, 3.34; Br, 22.06; N, 11.60; Found: C, 49.75; H, 3.34; Br, 22.05; N, 11.63]; LC/MS (ESI,  $m/z$ ): [M<sup>+</sup>], found 362.28, C<sub>15</sub>H<sub>12</sub>BrN<sub>3</sub>O<sub>3</sub> for 362.18.

### 2.2. Computational details

All calculations were made by Gaussian 03 software [22]. B3LYP method and 6-31G(d,p) basis set were used. X-ray structure coordinates were taken as starting point for calculations. No symmetry restrictions were applied. The optimized structures were taken as input for frequency calculations and for doing calculations in presence of solvent (CHCl<sub>3</sub> and DMSO) using polarized continuum model (PCM). No imaginary vibrations were detected so real energy minimum were obtained in all systems. Chemcraft [23] software is used to visualize the optimized structures. GaussView 4.1 [24] software was used to draw the frontier molecular orbitals (FMO) as well as the molecular electrostatic potential map (MEP). GIAO and TD-DFT methods were used to compute the NMR chemical shifts and the electronic spectra of the desired compound, respectively. CRYSTAL EXPLORER 3.1 program was used to perform the Hirshfeld surfaces theoretical analysis [25].

**Table 1**  
The crystal experimental data.

| Empirical formula  | C <sub>15</sub> H <sub>12</sub> BrN <sub>3</sub> O <sub>3</sub> |   |
|--|---|---|
| CCDC No.   | 1489664   |   |
| Formula weight   | 362.18  |   |
| Temperature  | 100 K   |   |
| Crystal system   | Triclinic   |   |
| Space group  | P-1   |   |
| Unit cell dimensions   | a = 7.9162 (5) Å<br>b = 11.4676 (7) Å<br>c = 15.3524 (8) Å      | $\alpha = 100.486 (2)^\circ$<br>$\beta = 96.305 (2)^\circ$<br>$\gamma = 90.753 (3)^\circ$ |
| Volume   | 1361.34 (14) Å <sup>3</sup>                                     |   |
| Z  | 4   |   |
| sin $\theta/\lambda$ max   | 0.671 (Å <sup>-1</sup> )  |   |
| Crystal size   | 0.32 × 0.28 × 0.06 mm <sup>3</sup>                              |   |
| No. of measured, independent and observed (i) reflections                | 35536, 6903, 5273   |   |
| Reflections collected  | 6903  |   |
| R(int)   | 0.099   |   |
| Absorption correction  | multi-scan SADABS Bruker 2014                                   |   |
| Restraints/parameters  | 1/401   |   |
| R[F <sup>2</sup> > 2 $\sigma$ (F <sup>2</sup> )], wR(F <sup>2</sup> ), S | 0.057, 0.138, 1.07  |   |
| $\Delta\rho_{\max}$ , $\Delta\rho_{\min}$                                | 1.66, -1.01 e.Å <sup>-3</sup>                                   |   |

## 3. Results and discussion

### 3.1. Chemistry

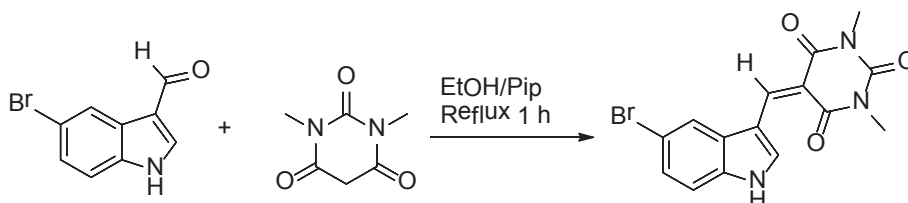
The 5-((5-Bromo-1H-indol-3-yl)methylene)-1,3-dimethylpyrimidine-2,4,6(1H,3H,5H)-trione was synthesized as shown in Scheme 1. The reaction proceeded smoothly when mixing of equimolar amount of substituted aldehyde and barbituric acid in EtOH under reflux in the presence of catalytic amount piperidine. The molecular structure of the later products was investigated by using different spectroscopic techniques such as <sup>1</sup>H, <sup>13</sup>C NMR, IR, TG/DTG, GCMS and X-ray single crystal technique.

### 3.2. X-ray crystal structure

A crystalline material was growing in a mixture of DCM/EtOH/Et<sub>2</sub>O at rt for 24 h. The molecular structure was solved by SHELXS-97 [26,27]. The crystal experimental data and selected geometric parameters of the desired compound are listed in Tables 1 and 2 respectively.

The unit cell of the 5-((5-Bromo-1H-indol-3-yl)methylene)-1,3-dimethylpyrimidine-2,4,6(1H,3H,5H)-trione contains two independent molecules. The chemical structure is indole ring (C1–C8/N1); and pyrimidine ring (C10/C11/N2/C13/N3/C15); which are bound together through the exo-double bond C9=C10 with bond lengths 1.369 (6) Å and 1.366 (5) Å in both molecules. The indole rings in the crystal structure make small dihedral angles 5.65° and 5.19° in both molecules which make the whole molecule nearly flat (Fig. 1).

The molecules are packed in the crystal structure with three classical hydrogen bonds between N–H...O and two non-classical hydrogen interactions between C–H...O (Fig. 2, Table 3).



**Scheme 1.** Synthesis of 5-((5-Bromo-1H-indol-3-yl)methylene)-1,3-dimethylpyrimidine-2,4,6(1H,3H,5H)-trione.

**Table 2**  
Geometric parameters (bond length (Å) and Angles (°)).

| Bond length   | Å         | Bond length   | Å         |
|---------------|-----------|---------------|-----------|
| Br1A–C4A      | 1.909 (5) | N2A–C11A      | 1.379 (5) |
| Br1B–C4B      | 1.913 (5) | N3A–C14A      | 1.469 (6) |
| O1A–C11A      | 1.233 (5) | N3A–C15A      | 1.394 (5) |
| O2A–C13A      | 1.218 (6) | N3A–C13A      | 1.385 (5) |
| O3A–C15A      | 1.237 (5) | N1B–C1B       | 1.398 (5) |
| O1B–C11B      | 1.226 (5) | N1B–C8B       | 1.330 (6) |
| O2B–C13B      | 1.209 (6) | N2B–C13B      | 1.380 (5) |
| O3B–C15B      | 1.221 (5) | N2B–C11B      | 1.388 (6) |
| N1A–C1A       | 1.387 (5) | N2B–C12B      | 1.468 (5) |
| N1A–C8A       | 1.351 (5) | N3B–C13B      | 1.413 (5) |
| N2A–C13A      | 1.389 (6) | N3B–C15B      | 1.379 (6) |
| N2A–C12A      | 1.464 (5) | N3B–C14B      | 1.484 (6) |
| Angle         | (°)       | Angle         | (°)       |
| C1A–N1A–C8A   | 110.1 (3) | O1A–C11A–N2A  | 119.0 (4) |
| C11A–N2A–C12A | 118.0 (3) | N2A–C13A–N3A  | 117.1 (4) |
| C11A–N2A–C13A | 124.1 (3) | O2A–C13A–N2A  | 121.7 (4) |
| C12A–N2A–C13A | 117.9 (3) | O2A–C13A–N3A  | 121.3 (4) |
| C13A–N3A–C14A | 115.3 (3) | N3A–C15A–C10A | 116.4 (4) |
| C13A–N3A–C15A | 124.9 (3) | O3A–C15A–C10A | 124.1 (3) |
| C14A–N3A–C15A | 119.6 (3) | O3A–C15A–N3A  | 119.5 (4) |
| C1B–N1B–C8B   | 111.2 (3) | N1B–C1B–C6B   | 130.3 (4) |
| C12B–N2B–C13B | 117.8 (4) | N1B–C1B–C2B   | 106.1 (3) |
| C11B–N2B–C12B | 116.9 (3) | Br1B–C4B–C3B  | 117.0 (3) |
| C11B–N2B–C13B | 125.3 (3) | Br1B–C4B–C5B  | 118.6 (3) |
| C14B–N3B–C15B | 118.1 (3) | N1B–C8B–C7B   | 109.5 (4) |
| C13B–N3B–C14B | 115.9 (3) | O1B–C11B–C10B | 123.5 (4) |
| C13B–N3B–C15B | 126.0 (3) | O1B–C11B–N2B  | 119.3 (4) |
| N1A–C1A–C6A   | 107.1 (3) | N2B–C11B–C10B | 117.2 (4) |
| N1A–C1A–C2A   | 130.2 (4) | O2B–C13B–N3B  | 122.0 (4) |
| Br1A–C4A–C5A  | 118.6 (3) | N2B–C13B–N3B  | 115.5 (4) |
| Br1A–C4A–C3A  | 118.0 (3) | O2B–C13B–N2B  | 122.5 (4) |
| N1A–C8A–C7A   | 109.8 (3) | N3B–C15B–C10B | 116.6 (4) |
| N2A–C11A–C10A | 117.4 (3) | O3B–C15B–N3B  | 118.2 (4) |
| O1A–C11A–C10A | 123.6 (3) | O3B–C15B–C10B | 125.3 (4) |

### 3.2.1. Hirshfeld surfaces analysis (HSA)

The HSA was carried out using crystal information CIF file output, as shown in Fig. 3. Intermolecular natural contacts can be cited as visual spots on the molecule surface photo. The strong contacts appeared as red large spots, while the weak one as small red spots [28–31]. Since the desired compound contains many of O and N donor-atoms with their free electrons, usually it can be easily detected by Hirshfeld surfaces due to the expected strong H-bonds formation. In the surface structure of the desired compound, eight sufficient red spots were detected per one molecule as seen in Fig. 3, which built 3D H-bonds network, as seen in Fig. 3d. On the

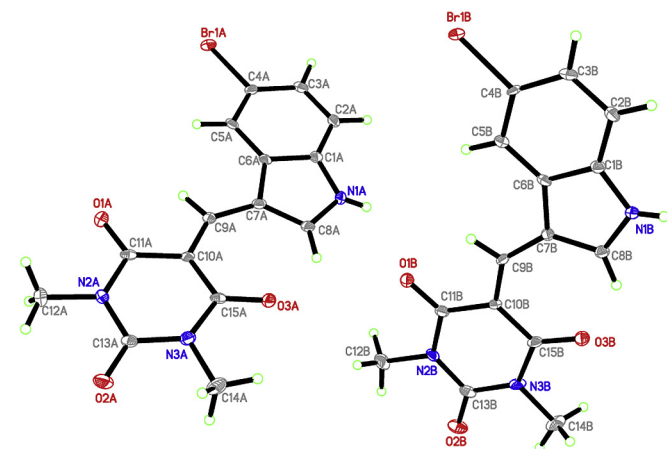


**Fig. 1.** ORTEP of the synthesized product.

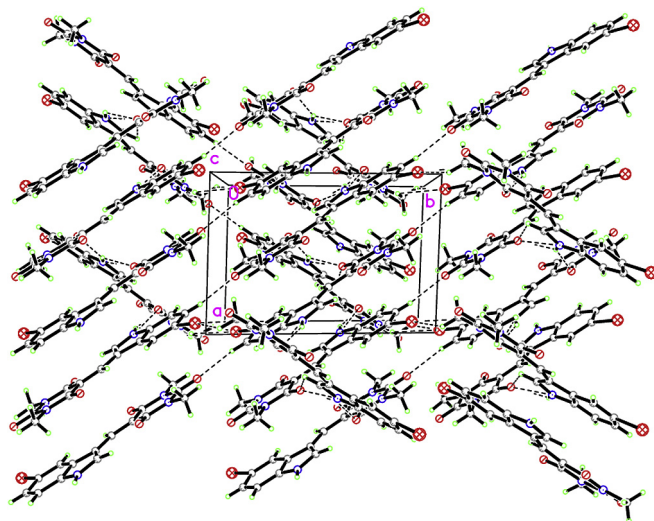


**Fig. 2.** View of the molecular packing in the compound. The N–H···O hydrogen bonds are shown as dashed lines.

$d_{norm}$ , the strongest H-bond type was cited to N–H···O=C, such bonds played a critical role in stabilizing the crystal structure of the desired compound in dimer form.

Fig. 4 illustrates the finger-print plot (FP), which highlights the important intermolecular contacts in the molecule. The FP analysis revealed that H···H intermolecular contacts as the largest contributor with a 34.6%. The 2D-FP plots over the Hirshfeld surfaces showed the presence of inter-contacts as follows: H···H > H···O > H···Br > H···C > H···N as depicted in Fig. 4.

### 3.3. DFT studies

#### 3.3.1. Optimized structure compared to XRD solved one

The calculated optimized structures of the desired compound and its H-bond dimer are given in Fig. 5, respectively. The bond distances and angles are given in Table 2 while the most important bond distances of the dimer are shown in Fig. 5.

The relative errors and relative error percentage (0.017 Å, 1.16%) in the calculated bond distances are quite small (Table 4). Moreover, the correlations between the calculated and experimental bond distances and angles are 0.9988 and 0.9968, respectively. Generally, the calculated geometry showed good agreement with the experimental one. The O2···H22 and O4···H20 intramolecular distances are calculated to be 2.212 and 2.033 Å in gas phase while experimentally observed at 2.263–2.267 Å and 2.097–2.173 Å, respectively. These results predicted the presence of some intramolecular C–H···O interactions where the O2···H22 is weaker than the O4···H20. Moreover, the calculations in solution were presented in

**Table 3**  
Hydrogen-bond geometry (Å, °).

| D–H···A                       | D–H    | H···A  | D···A     | D–H···A |
|-------------------------------|--------|--------|-----------|---------|
| N1A–H1AA···O1B                | 0.8800 | 2.2600 | 2.817 (4) | 121.00  |
| N1A–H1AA···O3B <sup>i</sup>   | 0.8800 | 2.4400 | 3.195 (4) | 145.00  |
| N1B–H1BA···O1A <sup>ii</sup>  | 0.8800 | 2.3800 | 2.925 (4) | 120.00  |
| N1B–H1BA···O3A <sup>iii</sup> | 0.8800 | 2.1300 | 2.912 (4) | 147.00  |
| C3A–H3AA···O2A <sup>iv</sup>  | 0.9500 | 2.3600 | 3.289 (6) | 167.00  |
| C8A–H8AA···O3A                | 0.9500 | 2.1700 | 2.850 (5) | 127.00  |
| C3B–H3BA···O2B <sup>v</sup>   | 0.9500 | 2.4600 | 3.386 (6) | 165.00  |
| C8B–H8BA···O3B                | 0.9500 | 2.1000 | 2.803 (6) | 130.00  |

Symmetry codes: (i)  $-x+1, -y+1, -z+1$ ; (ii)  $x, y, z+1$ ; (iii)  $-x+2, -y+1, -z+1$ ; (iv)  $x-1, y-1, z$ ; (v)  $x+1, y-1, z$ .

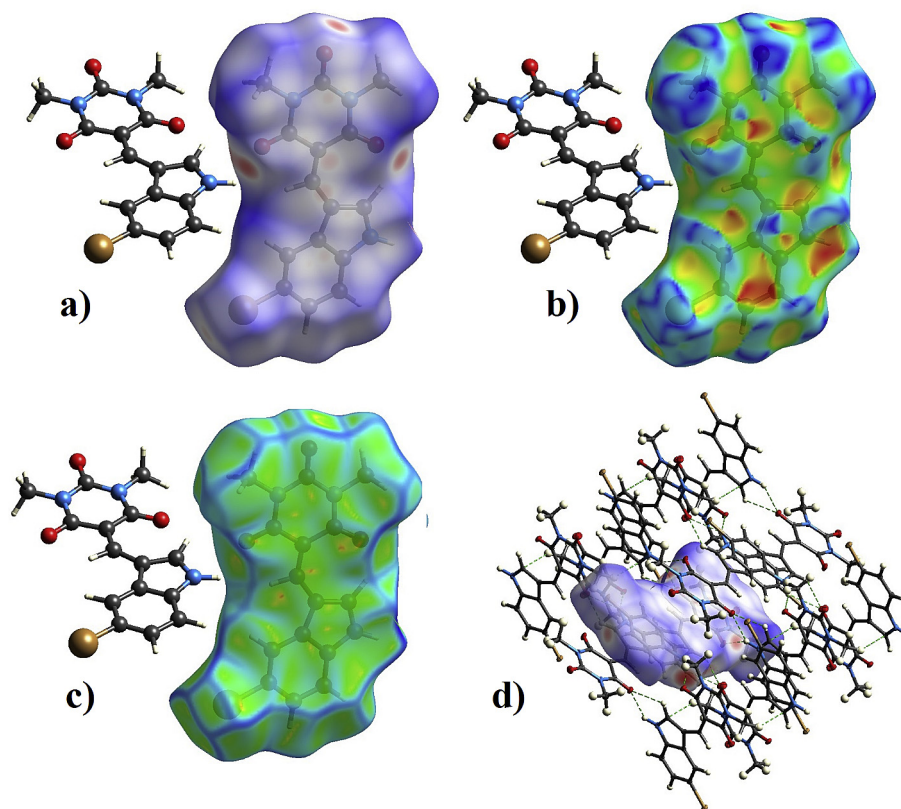


**Fig. 3.** a)  $d_{norm}$  mapped, b) shape index, c) curvedness and d) 3D H-Bonds network on Hirshfeld surface for visualizing the contacts. Colour-scale ranges between 0.16 au (blue) and 1.8 au (red). (For interpretation of the references to colour in this figure legend, the reader is referred to the web version of this article.)

presence of chloroform as solvent (Table 4). Almost the geometric parameters remained the same without significant variations except the N–H bond. This polar bond showed some elongation due to the solute-solvent interactions. The N–H bond distance is calculated to be 1.020 Å in solution instead of 1.008 Å in gas phase. In solution, the O2···H22 and O4···H20 intramolecular distances tend to be longer (2.221 Å and 2.067 Å, respectively) and the C–H···O interactions becomes weaker than those in the gas phase.

In case of the dimer, the intermolecular H-bonding interactions between two of desired compound significantly elongate the N–H and C=O bonds involved in this interaction while the rest of bonds remained almost unchanged. The N–H and C=O bonds in the free molecule are 1.008 and 1.226 Å, respectively instead of 1.020 and 1.236 Å in case of the dimer. There is elongation in these bonds by 0.012 and 0.010 Å, respectively. Interestingly, the dimer has two molecular units which are not exactly similar to each other which agree with the X-ray structure. In general, the bond distances obtained for the dimer structure have better agreement with the experimental results than those for the monomer. The presence of intermolecular interactions play important role in the accuracy of the DFT results when compared to the experimental solid state X-ray structure results.

### 3.3.2. MEP investigation

Molecular electrostatic potential map is a useful graph to present not only the electrophilic and nucleophilic sites of compound but also to recognize the most preferred sites for the H-bonding interactions (Fig. 6). The blue colored regions in our MEP indicated the electron poor regions (electrophile) while the red ones are the electron rich (nucleophile). The red and blue indicating the H-acceptor and H-donor sites for the H-bonding interactions. The

MEP graph shown in Fig. 6 indicated that the O-atoms and the NH proton are the most reactive nucleophile and electrophile, respectively. The O-atoms and the N–H proton are also, the best H-bond acceptor and H-bond donor sites, respectively.

### 3.3.3. Electronic spectra and TD-DFT calculations

The electronic spectra of the desired compound were measured in different solvents such as ethanol, acetonitrile and chloroform (Fig. 7). It is found that the solvent have almost negligible effect on the position of the spectral bands.

Table 5 showed the experimental maximum absorption wavelengths ( $\lambda_{max}$ ) of the most significant bands observed experimentally. In order to assign the origin of these electronic transitions we performed TD-DFT calculations at the optimized structure in gas phase and in presence of solvent such as chloroform. The polarized continuum model (PCM) was used to model the effect of solvation on the electronic spectra when compared to those in the gas phase. The assignments of the most important electronic transitions were collected also as shown in Table 5.

In chloroform, the studied compound showed seven electronic transitions. The longest wavelength band observed experimentally at 414 nm is calculated at 355.8 and 372.3 nm in gas phase and chloroform as solvent, respectively. This band showed bathochromic shift due to the solute-solvent interactions compared to the gas phase. This band is assigned to the electronic transition from HOMO to LUMO excitation (80%). The molecular orbital energy level diagram of the 414 nm transition band explained adequately the predicted bathochromic shift of this band in solution (Fig. 8). In presence of solvent the HOMO level is destabilized by 0.0964 eV and also the LUMO is destabilized by only 0.0201 eV. As a result the HOMO-LUMO energy gap is lowered and the



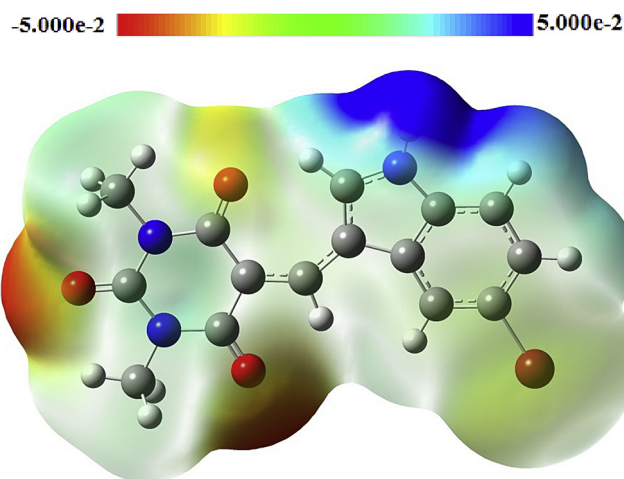


Fig. 6. The MEP graph.

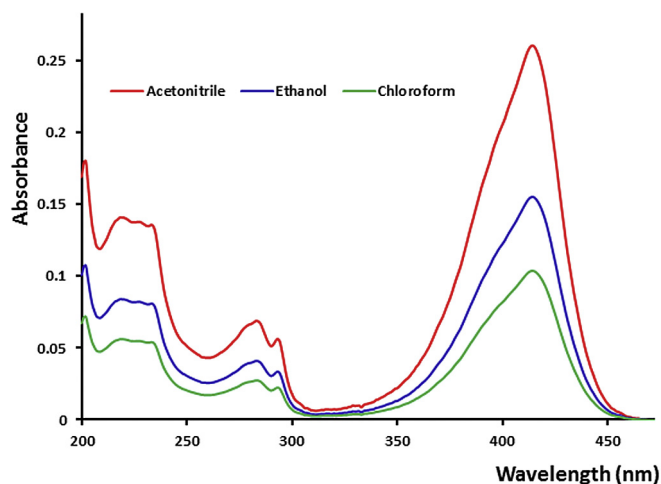


Fig. 7. The electronic spectra of the desired compound in different solvents.

### 3.3.4. Theoretical GIAO $^1\text{H}$ and $^{13}\text{C}$ NMR compared to experimental results

GIAO method is used to predict the  $^1\text{H}$  and  $^{13}\text{C}$  NMR chemical shifts of the desired compound both in gas phase and in DMSO solution, the results were compared with the experimental data. The calculated and experimental chemical shifts are given in Table 6. In gaseous state, the  $^{13}\text{C}$  NMR chemical shifts showed good correlation with the experimental results which are slightly improved when applied the solvent effects. In contrast, the  $^1\text{H}$  NMR has a correlation coefficient of 0.8562 in gas phase while in solution significant improvement takes place ( $R^2 = 0.9415$ ) due to solvent

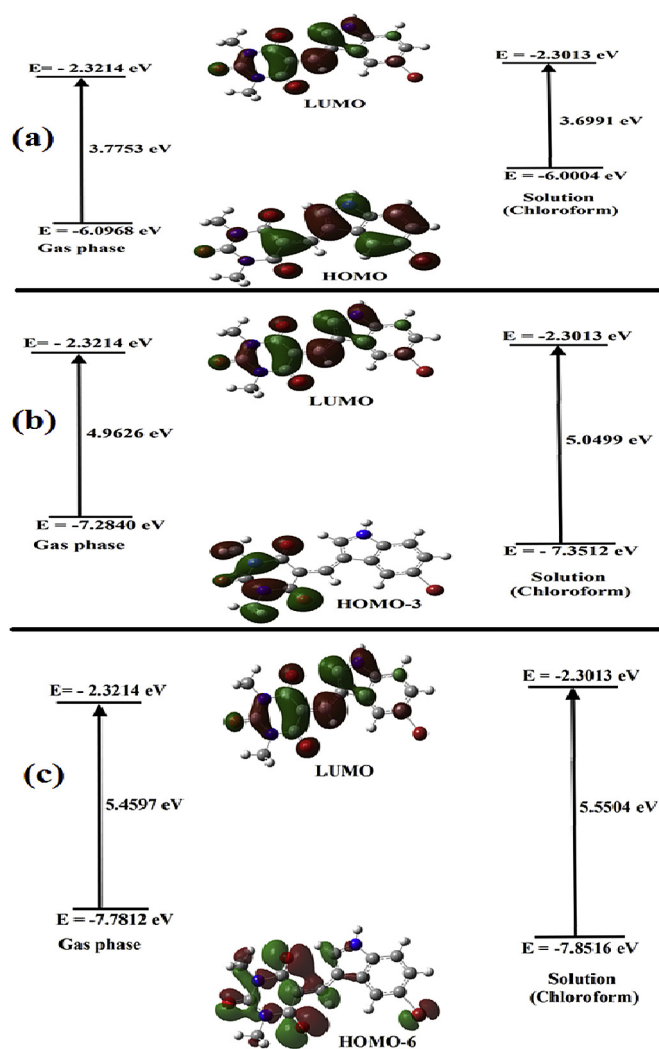


Fig. 8. The molecular orbital energy level diagram (a) HOMO→LUMO (calc. at 372.3 nm, exp. found at 414 nm in chloroform), (b) HOMO-3→LUMO (calc. at 285.5 nm, exp. at 295 nm in chloroform), (c) HOMO-6→LUMO (calc. at 278.2 nm, exp. at 285 nm in chloroform).

effect. The solvent correction for the  $^1\text{H}$  NMR chemical shifts is more valuable than  $^{13}\text{C}$  NMR.

### 3.4. TG/DTG investigation

Thermal TG/DTG analyses was performed to evaluate the thermal stability of the prepared trione compound in an open atmosphere condition, which was carried out over 0–600 °C temperature range and 10 °C/min heat rate, as seen in Fig. 9. The

Table 5

The experimental, calculated  $\lambda_{\text{max}}$  (nm) and oscillator strength (f) of the most important electronic transitions.

| Gas                         |        | Chloroform                  |        | Assignment (CHCl <sub>3</sub> )            | Experimental $\lambda_{\text{max}}$ (nm) |
|-----------------------------|--------|-----------------------------|--------|--|--|
| $\lambda_{\text{max}}$ (nm) | f      | $\lambda_{\text{max}}$ (nm) | f      |  |  |
| 355.8                       | 0.5256 | 372.3                       | 0.7460 | H→L (80%)                                  | 414                                      |
| 290.5                       | 0.0034 | 285.8                       | 0.0044 | H-3→L (95%)                                | 295                                      |
| 284.0                       | 0.0002 | 278.2                       | 0.0002 | H-6→L (90%)                                | 285                                      |
| 230.8                       | 0.0001 | 234.4                       | 0.0001 | H-1→L+3 (24%), H→L+3 (71%)                 | 235                                      |
| 226.9                       | 0.0073 | 226.6                       | 0.0063 | H-9→L (93%)                                | 229                                      |
| 213.9                       | 0.2722 | 214.1                       | 0.4248 | H-1→L+1 (14%), HOMO→L+2 (48%)              | 219                                      |
| 205.6                       | 0.0209 | 207.4                       | 0.0269 | H-10→L (12%), H-4→L+1 (25%), H-1→L+2 (48%) | 203                                      |

**Table 6**

The calculated chemical shifts in gas phase and DMSO solvent compared to the experimental data.

| Atom                 | Calculated    |               | Exp.   | Atom                 | Calculated    |               | Exp.  |
|----------------------|---------------|---------------|--------|----------------------|---------------|---------------|-------|
|                      | gas           | DMSO          |        |                      | gas           | DMSO          |       |
| C9                   | 121.09        | 130.97        | 135.70 | H6                   | 7.93          | 10.03         | 12.86 |
| C10                  | 99.30         | 110.91        | 127.90 | H11                  | 7.37          | 7.83          | 7.46  |
| C12                  | 115.19        | 123.17        | 130.40 | H13                  | 7.55          | 7.64          | 7.55  |
| C14                  | 125.92        | 132.32        | 122.50 | H16                  | 8.28          | 8.16          | 8.01  |
| C15                  | 110.28        | 116.95        | 128.70 | H20                  | 10.47         | 10.04         | 8.69  |
| C17                  | 119.87        | 127.76        | 132.20 | H22                  | 9.19          | 8.87          | 9.50  |
| C18                  | 104.46        | 111.50        | 115.30 | H26                  | 3.12          | 2.92          | 3.46  |
| C19                  | 127.02        | 138.32        | 134.70 | H27                  | 4.43          | 4.11          | 3.46  |
| C21                  | 133.62        | 141.95        | 142.10 | H28                  | 3.12          | 2.91          | 3.46  |
| C23                  | 102.14        | 107.76        | 133.10 | H31                  | 4.70          | 4.45          | 3.46  |
| C24                  | 149.12        | 159.02        | 194.90 | H32                  | 2.99          | 2.78          | 3.46  |
| C25                  | 21.93         | 29.77         | 35.40  | H33                  | 2.99          | 2.77          | 3.46  |
| C29                  | 136.83        | 146.09        | 163.50 | <b>R<sup>2</sup></b> | <b>0.8562</b> | <b>0.9415</b> |       |
| C30                  | 20.68         | 28.48         | 35.40  |                      |               |               |       |
| C34                  | 148.56        | 156.87        | 177.90 |                      |               |               |       |
| <b>R<sup>2</sup></b> | <b>0.9617</b> | <b>0.9633</b> |        |                      |               |               |       |

**Bold** for correlation coefficients.

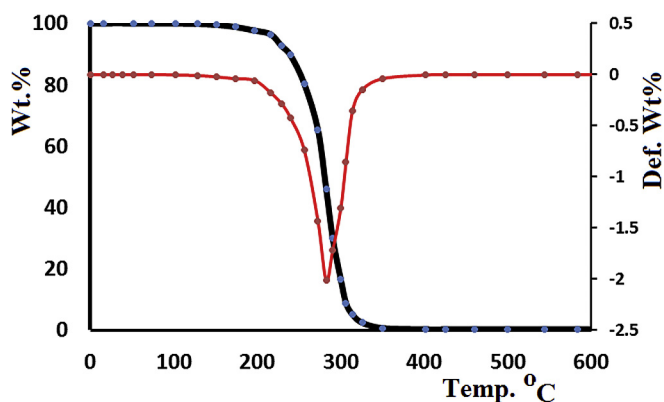


**Fig. 9.** TG-DTG of the desired compound.

desired organic compound  $C_{15}H_{12}BrN_3O_3$  displayed a good thermal stability from 0 to 215 °C, the thermal decay started after 215 °C and ended to 350 °C with 100% mass loss. Therefore, the trione undergoes one-step thermal decomposition without intermediate. Mostly, the compound was decomposed to light oxide gases such as:  $H_2O$ ,  $NO_2$ ,  $CO_2$  and  $BrO_3$ .

#### 4. Conclusions

The 5-((5-bromo-1*H*-indol-3-yl)methylene)-1,3-dimethylpyrimidine-2,4,6(1*H*,3*H*,5*H*)-trione has been synthesized under reflux condition and physicochemical characterized. Molecular structure of the desired compound is solved to an accuracy of  $R = 0.057$  by X-ray technique. The optimized structures of the monomer and dimer molecule were calculated using DFT B3LYP/6-31G(d,p) method then compared with the experimental results. The calculated bond distances and angles were found to agree with the experimental X-ray structure data. The effects of intermolecular H-bonding interactions on the geometric and electronic properties were compared where the dimer showed better accuracy with the experimental data than the monomer. The suitable sites for H-bonding interactions were determined using Hirshfeld surface analysis and MEP map, which revealed the N–H as H-donor and the O=C as H-acceptor forming the N–H...O=C as shortest H-bond dimerized two molecules. The electronic spectra were

measured, assigned and computed, the longest wavelength band observed experimentally at 414 nm was assigned to the electronic transition from HOMO to LUMO excitation (80%). This band showed bathochromic shift in solution compared to the gas phase because the solvent destabilized the HOMO level by 0.0964 eV and LUMO by only 0.0201 eV which decrease the transition energy. In contrast, the two shorter wavelength bands (cal. 290.5 and 284.0) were found to undergo hypsochromic shift in solution which are adequately explained using molecular orbital energy level analysis. The NMR chemical shifts were calculated using GIAO method and results were found in good agreement with the experimental data. The desired compound displayed a good thermal stability and one step thermal decomposed mechanism.

#### Acknowledgements

The authors are thankful to King Saud University, Deanship of Scientific Research, College of Science Research Center, for financial support of this project.

#### References

- [1] S. Budavari, M.J. O'Neil, A. Smith, P.E. Heckelman, The Merck Index, Merck & Co. Inc., Rahway, NJ, 1989, p. 1008.
- [2] J.S. Biradar, B.S. Sasidhar, R. Parveen, Synthesis, antioxidant and DNA cleavage activities of novel indole derivatives, *Eur. J. Med. Chem.* 45 (2010) 4074–4078.
- [3] R.K. Behera, A.K. Behera, R. Pradhan, A. Pati, M. Patra, Studies on spiroheterocycles, part III: synthesis of diazaspiroindecanetetraone derivatives containing biologically active heterocycles, *Phosphorus Sulfur Silicon Relat. Elem.* 184 (2009) 753–765.
- [4] W.G. Brouwer, E.E. Felauerand and A.R. Bell, U.S. Patent 779 982 990, *Chem. Abstr.* 114 (1991) 185539.
- [5] I. Chen, S. Safe, L. Bjeldanes, Indole-3-carbinol and diindolylmethane as aryl hydrocarbon (Ah) receptor agonists and antagonists in T47D human breast cancer cells, *Biochem. Pharmacol.* 51 (1996) 1069–1076.
- [6] S. Suzen, E. Buyukbingol, Anti-cancer activity studies of indolalithiohydantoin (PIT) on certain cancer cell lines, *Il Farm.* 55 (2000) 246–248.
- [7] E. Buyukbingol, S. Suzen, G. Klopman, Studies on the synthesis and structure-activity relationships of 5-(3'-indolal)-2-thiohydantoin derivatives as aldose reductase enzyme inhibitors, *Farmaco* 49 (1994) 443–447.
- [8] S. Suzen, E. Buyukbingol, Evaluation of anti-HIV activity of 5-(2-phenyl-3'-indolal)-2-thiohydantoin, *Il Farm.* 53 (1998) 525–527.
- [9] Y.J. Chyan, B. Poeggeler, R.A. Omar, D.G. Chain, B. Frangione, J. Ghiso, M.A. Pappolla, Potent neuroprotective properties against the Alzheimer  $\beta$ -amyloid by an endogenous melatonin-related indole structure, indole-3-propionic acid, *J. Biol. Chem.* 274 (1999) 21937–21942.
- [10] P.M. Liebmann, A. Wölfler, P. Felsner, D. Hofer, K. Schauenstein, Melatonin and the immune system, *Int. Arch. Allergy. Immunol.* 112 (1997) 203–211.
- [11] D. Pagé, H. Yang, W. Brown, C. Walpole, M. Fleurent, M. Fyfe, F. Gaudreault, S. St-Onge, New 1, 2, 3, 4-tetrahydropyrrrolo [3, 4-b] indole derivatives as selective CB2 receptor agonists, *Bioorg. Med. Chem. Lett.* 17 (2007) 6183–6187.
- [12] M.A. Radwan, E.A. Ragab, N.M. Sabry, S.M. El-Shenawy, Synthesis and biological evaluation of new 3-substituted indole derivatives as potential anti-inflammatory and analgesic agents, *Bioorg. Med. Chem.* 15 (2007) 3832–3841.
- [13] W.O. Foye, Principles of Medicinal Chemistry, Lea & Febiger, London, 1989, p. 159.
- [14] D.J. Guerin, D. Mazeas, M.S. Musale, N.F.M. Naguib, O.N. Al Safarjalani, M.H. el Kouni, R.P. Panzica, Uridine phosphorylase inhibitors: chemical modification of benzyloxybenzyl-barbituric acid and its effects on urdpase inhibition, *Bioorg. Med. Chem. Lett.* 9 (1999) 1477–1480.
- [15] L.S. Goodman, A. Gilman, in: The Pharmacological Basis of Therapeutics, Mc Graw-Hill, New Delhi, 1991, pp. 358–360.
- [16] R.J. Sundberg, Indoles, Academic Press, San Diego, 1996, p. 113.
- [17] G.M. Ziarani, F. Aleali, N. Lashgari, Recent applications of barbituric acid in multicomponent reactions, *RSC Adv.* 6 (2016) 50895–50922.
- [18] A. Barakat, M.S. Islam, A.M. Al-Majid, H.A. Ghabbour, S. Yousuf, M. Ashraf, N.N. Shaikh, M.I. Choudhary, R. Khalil, Z. Ul-Haq, Synthesis of pyrimidine-2, 4, 6-trione derivatives: anti-oxidant, anti-cancer,  $\alpha$ -glucosidase,  $\beta$ -glucuronidase inhibition and their molecular docking studies, *Bioorg. Chem.* 68 (2016) 72–79.
- [19] A. Barakat, A.M. Al-Majid, H.J. Al-Najjar, Y.N. Mabkhot, H.A. Ghabbour, H.K. Fun, An efficient and green procedure for synthesis of rhodanine derivatives by aldol-thia-Michael protocol using aqueous diethylamine medium, *RSC Adv.* 4 (2014) 4909–4916.
- [20] A.M. Al-Majid, A. Barakat, H.J. Al-Najjar, Y.N. Mabkhot, H.A. Ghabbour, H.K. Fun, *Int. J. Mol. Sci.* 14 (2013) 23762–23773.

- [21] A. Barakat, A.M. Al-Majid, M.S. Islam, M. Ali, S.M. Soliman, M.R.H. Siddiqui, H.A. Ghabbour, H.K. Fun, Molecular structure investigation and tautomerism aspects of (E)-3-benzylideneindolin-2-one, *J. Chem. Sci.* 127 (2015) 1547–1556.
- [22] M. Frisch, G.W. Trucks, H. Schlegel, G.E. Scuseria, M.A. Robb, J.R. Cheeseman, J.M. Millam, Gaussian 03, Revision C. 02, vol. 4, Gaussian, Inc., Wallingford, CT, 2004.
- [23] R. Ennington, T. Keith, J. Millam, Shawnee Mission KS, GaussView, Version, 5, Semichem Inc, 2009.
- [24] Chemcraft 1.6 software, <http://www.chemcraftprog.com>.
- [25] S.K. Wolff, D.J. Grimwood, J.J. McKinnon, D. Jayatilaka, M.A. Spackman, Crystal explorer 2.1, University of Western Australia, Perth, 2007.
- [26] G.M. Sheldrick, A short history of SHELX, *Acta Cryst.* 64 (2008) 112–122.
- [27] A.L. Spek, Structure validation in chemical crystallography, *Acta Cryst.* 65 (2009) 148–155.
- [28] M.A. Spackman, D. Jayatilaka, Hirshfeld surface analysis, *Cryst. Eng. Comm.* 11 (2009) 19–32.
- [29] M.A. Spackman, J.J. McKinnon, Fingerprinting intermolecular interactions in molecular crystals, *Cryst. Eng. Comm.* 4 (2002) 378–392.
- [30] I. Warad, F. Al-Rimawi, A. Barakat, S. Affouneh, N. Shivalingegowda, N.K. Lokanath, I.M. Abu-Reidah, Synthesis, spectral, thermal, crystal structure, Hirshfeld analysis of, [bis(triamine) Cadmium(II)][Cadmium(IV)tetra-bromide]complexes and their thermolysis to CdO nanoparticles, *Chem. Cen. J.* 10 (2016) 1–11.
- [31] I. Warad, A. Barakat, Synthesis, physicochemical analysis of two new hemilabile ether-phosphine ligands and their first stable bis-ether-phosphine/cobalt(II) tetrahedral complexes, *J. Mol. Struct.* 1134 (2017) 17–24.